applied sciences

MDPI

Article

Spatio-Temporal Variation of Reference Evapotranspiration and Its Climatic Drivers over the Tibetan Plateau during 1970–2018

Shanshan Hu [1], Ruyi Gao [1], Tao Zhang [2,*], Peng Bai [3] and Rui Zhang [2,*]

[1] Beijing Laboratory of Water Resources Security, College of Resource Environment and Tourism, Capital Normal University, Beijing 100048, China; hushanshan@cnu.edu.cn (S.H.); 2180902129@cnu.edu.cn (R.G.)
[2] Land Satellite Remote Sensing Application Center (LASAC), Beijing 100048, China
[3] Key Laboratory of Water Cycle & Related Land Surface Process, Institute of Geographic Sciences and Natural Resources Research, Chinese Academy of Sciences, Beijing 100101, China; baip@igsnrr.ac.cn
* Correspondence: zhangt@lreis.ac.cn (T.Z.); zhangrui@radi.ac.cn (R.Z.)

Abstract: Reference evapotranspiration (ET_0) is a key component of hydrologic cycle and it is important for water resources management. Analysis of ET_0 changes is particularly critical for understanding the impacts of climatic change on hydrology in ecologically fragile regions. In this study, using the Penman–Monteith method and the Mann–Kendall test, the variation characteristics of ET_0 on the Tibetan Plateau (TP) from 1970 to 2018 was analyzed, and the dominant climatic factors controlling the change of ET_0 was also explored. The result shows that in TP region: (1) there was an abrupt change in the trend of ET_0 around 1997, and the ET_0 declined at a rate of −25.9 mm/decade during 1970–1996 but increased by 31.1 mm/decade during 1997–2018; (2) ET_0 is most sensitive to solar radiation, then relative humidity, wind speed and mean temperature; (3) the decrease of ET_0 before 1997 was mainly due to the decline of wind speed and the increase of relative humidity, while the increase of ET_0 after 1997 was mainly due to the decrease of relative humidity. The results of this study can provide data reference for the research of water balance on the TP.

Keywords: Tibetan Plateau; reference evapotranspiration; climate change; dominant factors

Citation: Hu, S.; Gao, R.; Zhang, T.; Bai, P.; Zhang, R. Spatio-Temporal Variation of Reference Evapotranspiration and Its Climatic Drivers over the Tibetan Plateau during 1970–2018. *Appl. Sci.* **2021**, *11*, 8013. https://doi.org/10.3390/app11178013

Academic Editors: Francisco Barraza and Nathan J. Moore

Received: 2 July 2021
Accepted: 26 August 2021
Published: 30 August 2021

1. Introduction

As a link between water balance and surface energy balance [1], evapotranspiration is an important index reflecting climate variation and water circulation [2,3]. Reference evapotranspiration (ET_0) represents the maximum amount of evapotranspiration from a hypothetical reference surface under specific climatic conditions, given an adequate supply of water [4]. ET_0 plays a critical role in irrigation management [5] and is also an important parameter for agriculture water demand estimation and water balance analysis [6]. The Penman–Monteith (P-M) method is a fairly reliable method to estimate ET_0, which considers radiative and aerodynamic terms [7]. It focuses on the meteorological factors controlling evaporation process and is widely used in numerous research [8,9]. Understanding the spatial–temporal changes in ET_0 and the main causes can provide considerable understanding into the impact of climatic variation on water resources and hydrological cycles [10].

Extensive research has explored the spatial variation characteristics of ET_0 and the impact of climate factors on ET_0 in the late years [11]. It reported that pan-evaporation and ET_0 both have shown a steady downward trend in many regions of the world over the past several decades, including China, India, New Zealand and Italy [12–15], which is called 'evaporation paradox' [16]. The reasons for decreasing ET_0 have been widely discussed, global dimming and wind stilling were usually employed to explain the changes. For example, Han et al. [17] analyzed the entire trend in ET_0 in Jing-Jin-Ji region, finding that the decrease of wind speed and sunshine hours offset the influence of increased air temperature and led to a reduction in ET_0 before 1992. Xu et al. [18] found downward

trends in ET_0 in the Yellow River and the reduction of wind speed was the major driving force for decreasing trends. However, in recent years, increased ET_0 has been found in some regions, such as India and China [19]. Investigating long term change in ET_0 over India's humid tropical Narmada River watershed, Pandey et al. [20] found an increasing trend in ET_0. Cong et al. [21] found that annual pan evaporation in China has increased since 1986. The changes in climatic variables such as air temperature, wind speed may explain the increase of ET_0. The increase of pan evaporation in China is mainly owing to the increase of vapor pressure deficit [21]. Liu et al. [22] investigated the ET_0 trends in the Northwest China from 1960 to 2010, finding the ET_0 began to increase in 1994, mainly caused by the increasing atmospheric temperature and wind speed. Since there are many factors affecting ET_0, the temporal and spatial differences between its changes and the changes of climate factors are complex and diverse. In addition, it is still uncertain how much ET_0 changes are caused by a certain factor. Therefore, it is necessary to further study the variation of ET_0 and its possible causes.

The Tibetan Plateau (TP), as the 'third pole' of the earth, is very sensitive to global change due to its unique climate conditions and natural environment [23]. The TP is rich in lakes, glaciers, and wetlands and is the main source area of several major rivers in Asia. The management of affluent water resources on the plateau are not only a major issue related to China, but also the neighboring countries located in the lower reaches of the international rivers originating from the plateau. The management of abundant water ET_0 is the key constituent of the hydrologic cycle and has a great impact on regional water resources. Several studies have focused on the variation of ET_0 over the TP under the background of climatic change [3,24,25]. Zhang et al. [26] pointed out that the decrease of wind speed and sunshine duration were the dominant factors for the significant decline of ET_0 in the northern and southeastern TP from 1971 to 2004. Wang et al. [27] pointed out that ET_0 increased from 1997 to 2014 and the reduction of relative humidity played a crucial role in increasing of ET_0. This study will analyze and quantify the possible abrupt change characteristics of ET_0 and the impact of climatic factors on ET_0 during different stages over the TP.

This paper focused on the following objectives: (1) to analyze the temporal–spatial trends and transition characteristics of ET_0 from 1970 to 2018 on the TP region; (2) to investigate the temporal–spatial variation characteristics of climatic variables controlling the evaporation process; (3) to identify the main climate reasons for ET_0 change in different stages. The findings can improve the understanding of climate change impacts on ET_0 and provide useful information for water resources management and sustainable development.

2. Materials and Methods

2.1. Study Area

The TP is the largest geomorphologic unit on the Eurasian continent, ranging from 25°–40° N and 75°–105° E, covering most of the Tibet Autonomous Region and Qinghai Province in western China, with a total area of more than 2.5 million km^2 (Figure 1). The TP is the highest and most extensive plateau in the world, known as the 'roof of the world', with about 56% of the region over 4000 m above sea level [28]. Due to its high altitude and large volume, it forms a unique 'plateau climate'. The annual average temperature of the TP is reduced from 20 °C in the southeast to below −6 °C in the northwest. The annual precipitation is also reduced from 2000 mm to below 50 mm. The main vegetation cover in this area is grassland and forest. The grassland is mainly divided into alpine meadow, alpine grassland and alpine desert [29].

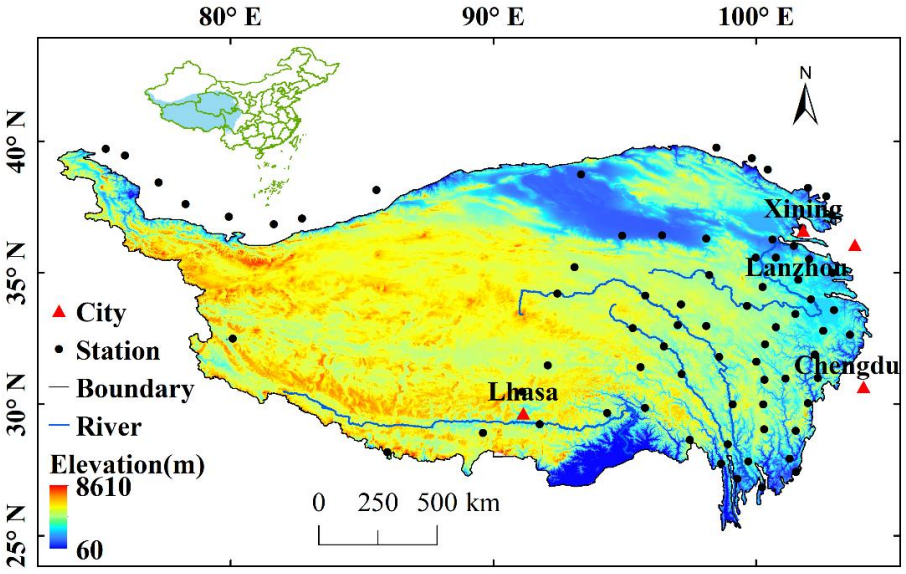

Figure 1. Location of the study area and the distribution of meteorological stations.

2.2. Data Sources

Daily meteorological records from 73 meteorological stations in and around the TP during the period 1970–2018 were used in this study and the altitude of these stations ranges from 1231.2 to 4645.1 m. The meteorological data includes daily average air temperature, maximum air temperature, minimum air temperature, relative humidity, wind speed, air pressure, sunshine duration and the 20 cm pan evaporation. These datasets were provided by the China Meteorological Data Service Center (CMDC) (http://data.cma.cn/, accessed on 6 May 2019) and were processed with quality control. The 90 m DEM data set of the TP is provided by Geospatial Data Cloud site, Computer Network Information Center, Chinese Academy of Sciences (http://www.gscloud.cn, accessed on 12 August 2019).

2.3. Methods

2.3.1. Calculation of ET_0

Penman–Monteith (P-M) formula was used to estimate daily ET_0 in this article which was proposed by the FAO (Food and Agriculture Organization). The P-M method estimates ET_0 from hypothetical reference grass with an assumed height of 0.12 m, a fixed surface resistance of 70 m·s^{-1}, and an albedo of 0.23 [30]. The formula is:

$$ET_0 = \frac{0.408\Delta(R_n - G) + \gamma \frac{900}{T_{mean}+273} U_2(e_s - e_a)}{\Delta + \gamma(1 + 0.34U_2)} \quad (1)$$

where ET_0 is the daily reference evapotranspiration (mm/d), Δ is the slope of the vapor pressure curve and γ is the psychometric constant (kPa/°C), R_n is the net radiation and G is the soil heat flux density (MJ·m^{-2}·day^{-1}), T_{mean} is the mean air temperature (°C), U_2 is the wind speed at 2 m height (m/s), e_s is the saturation vapor pressure and e_a is the actual vapor pressure (kPa).

Reference evapotranspiration and pan evaporation both represent evaporative capacity of a basin under certain climatic conditions and their good relationship had been manifested by previous research [31]. The pan coefficient and correlation between them were calculated to verify the applicability of the P-M model (Figure 2). The correlation coefficient between pan evaporation and reference evapotranspiration was 0.71 with a pan coefficient of 1.75, which indicates that the P-M model is suitable for the analysis of reference evapotranspiration on the TP.

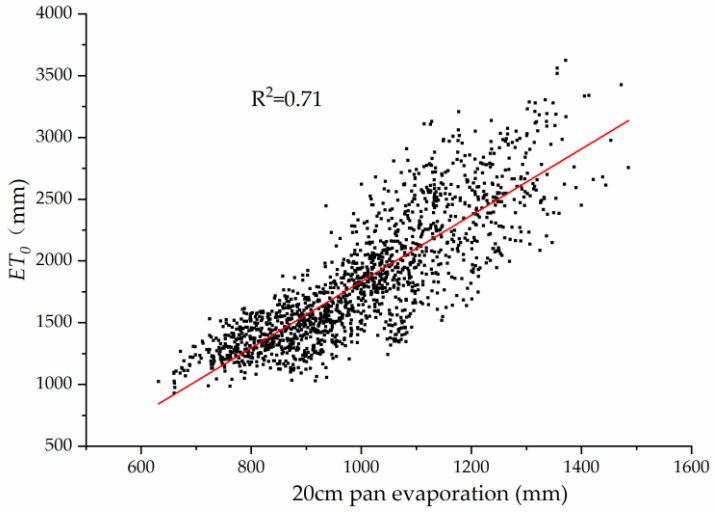

Figure 2. The relationship between P-M ET_0 and the 20 cm pan evaporation.

2.3.2. Cramer Test for Abrupt Change Point

The Cramer test is used to detect the mutation of ET_0 series. Cramer's test has displayed fine performance in checking the stabilization of records by comparing the whole average value of the record and the means of certain parts of the record [32]. The Cramer's test statistic t_k is calculated as follows:

$$t_k = \sqrt{\frac{n(N-2)}{N - n\left(1+\tau_k^2\right)}} \times \tau_k \tag{2}$$

$$\tau_k = \frac{\overline{x}_k - \overline{x}}{S}, \overline{x}_k = \frac{1}{n}\sum_{i=k+1}^{k+n} x_i, \overline{x} = \frac{1}{N}\sum_{i=1}^{N} x_i \tag{3}$$

where $\overline{x}$ and S are the mean and standard deviation, for the entire period of N years, and $\overline{x}_k$ is the mean of the sub period of the n years to be compared with $\overline{x}$.

2.3.3. Mann–Kendall Test for Trend Analysis

The Mann–Kendall (MK) test is used to analyze ET_0 and climate factors trends. This method does not need to consider the distribution form of the detection sequence, and can exclude the influence of individual extreme values on the sequence test, which is suitable for testing the trend change of time series of meteorological, hydrological and other types of variables [32,33]. It is highly recommended for general use by the World Meteorological Organization [34]. Its principle is as follows: the original assumption is that H_0 is n (x_1, x_2, ..., x_n) independent time series samples with the same distribution; alternative hypothesis H_1 is a bilateral test, the statistical value S is calculated as follows [17]:

$$S = \sum_{i=2}^{n}\sum_{j-1}^{i-1} sign(X_i - X_j) \tag{4}$$

$$sign\left(X_i - X_j\right) = \begin{cases} 1 & X_i - X_j > 0 \\ 0 & X_i - X_j = 0 \\ -1 & X_i - X_j < 0 \end{cases} \tag{5}$$

where: any $i \neq j$, $i \leq n$, $j \leq n$, when S approximately obeys normal distribution, and the trend test statistical value Z is obtained by means of S standardization processing:

$$Z = \begin{cases} \frac{S-1}{\sqrt{Var(S)}} & S > 0 \\ 0 & S = 0 \\ \frac{S+1}{\sqrt{Var(S)}} & S < 0 \end{cases} \quad (6)$$

If $|Z| > Z_{1-\alpha/2}$, the null hypothesis is rejected with a given confidence level α; namely, there is a significant trend in the time series data. When α is equal to 0.05, $Z_{1-\alpha}$ is equal to 1.96, respectively. The Z value is used to assess the statistics trend; a positive Z value expresses an upward trend, a negative Z value expresses a downward trend.

The annual change rate of data is evaluated by the least square method. The principle is to look for the best function matching of data by minimizing the square sum of errors [35].

2.3.4. Spatial Interpolation Method

Spatial interpolation is very important for obtaining the spatial distribution characteristics of climate variables when meteorological stations are few and widely separated. In this paper, the gradient plus inverse distance squared (GIDS) method is used for interpolating climate variables and ET_0 [36]. It is an inverse distance weighting method that takes into account the changes of meteorological factors with latitude, longitude and altitude. Previous studies have shown that this method has good applicability in areas with large terrain undulations and uneven site distribution [37]. The interpolating climate variable is calculated as follows [36,37]:

$$Z = [\sum_{i=1}^{N} \frac{Z_i + (X - X_i) \times C_x + (Y - Y_i) \times C_y + (E - E_i) \times C_e}{d_i^2}] / [\sum_{i=1}^{N} \frac{1}{d_i^2}] \quad (7)$$

where Z is the estimated climatic variable, Z_i is the value at climate station i, d_i is the distance from the site to climate station i and N is the number of climate stations used for the interpolation. X, Y and E are the longitude, latitude, and altitude of the point to be estimated, respectively, X_i, Y_i and E_i are the longitude, latitude, and altitude of climate station i, respectively, and C_x, C_y and C_e are regression coefficients for X, Y and E, respectively.

The daily ET_0 of 73 meteorological stations on the TP in 1970–2018 is calculated and transformed into ET_0 at annual scale. The annual average ET_0 on the TP is obtained by interpolating the annual ET_0 of 73 stations to the centroid of the area using the GIDS method.

2.3.5. Sensitivity Analysis and Contribution Rate Calculation

The sensitivity coefficient method is used to analyze the sensitivity of climate factors to ET_0 quantitatively [38]. The commonly used sensitivity analysis method is to assume that other variables are fixed, and to evaluate the impact of a variable change on the model output. The sensitivity coefficient of the ET_0 to a climate variable x is defined by [39,40]:

$$S_x = \lim_{\Delta x \to 0} \left(\frac{\Delta ET_0 / ET_0}{\Delta x / x} \right) = \frac{\partial ET_0}{\partial x} \cdot \frac{x}{ET_0} \quad (8)$$

A first-order Taylor series approximation was applied to calculate S_x [41,42]:

$$S_x = \frac{\Delta ET_0}{\Delta x} \cdot \frac{x}{ET_0} \quad (9)$$

where S_x is the sensitivity coefficient of the climate variable x, Δx is the relative change of climate factor x, and ΔET_0 is the relative change in ET_0 induced by Δx.

In this study, ET_0 was recalculated by making a ±10% change to each meteorological factors (solar radiation (RS), relative humidity (RH), air temperature (T_{mean}) and wind speed (U_2)) while keeping the other factors constant; sensitivity coefficient S_x was calculated from Equation (9). A positive value of S_x indicates that ET_0 increases as x increases, and vice versa. The greater the absolute value of the sensitivity coefficient, the greater the effect of the variable on ET_0.

The sensitivity coefficient reflects the influence of meteorological variables on ET_0, but it is not equal to the ET_0 change caused by a certain variable. Here, the contribution rate is introduced to analyze the change of ET_0 caused by a single meteorological factor. It is the product of the sensitivity coefficient of a climate factor and its multi-year change rate [11]. A positive contribution means that the variety of a meteorological factor has a positive effect on the variety of ET_0 and vice versa. The larger the absolute value is, the greater the impact on ET_0 will be. The contribution rate was calculated using the following formulas [43,44]:

$$CR_x = S_x \cdot RC_x \tag{10}$$

$$RC_x = \frac{n \cdot a_x}{\overline{x}} \times 100\% \tag{11}$$

where CR_x is the contribution rate climate variable x to ET_0; RC_x is the multi-year change rate of x; n is the number of years; a_x represents the trend rate of meteorological factor x during the corresponding study period; $\overline{x}$ is the multi-year absolute average value of x during the evaluation period. In this paper, we calculated the sensitivity of ET_0 to RS, RH, T_{mean} and U_2, and calculated the contribution rate of these four climatic factors to ET_0. The evaluation period includes three periods: during the period from 1979 to 2018 and two periods before and after the mutation point.

$$C\_(ET_0) = CR_{RS} + CR_{RH} + CR_{Tmean} + CR_{U2} + \varepsilon \tag{12}$$

where CR_{RS}, CR_{RH}, CR_{Tmean}, CR_{U2} are the individual contributions to the long-term trend in ET_0 as a result of the change in RS, RH, T_{mean} and U_2, respectively. $C\_(ET_0)$ is the sum of the contribution of variation in RS, RH, T_{mean} and U_2 to the change in ET_0. ε is the error between $C(ET_0)$ and ET_0 trend calculated by P-M model ($LR\_(ET_0)$).

3. Results

3.1. Spatio-Temporal Variation Characteristics of ET_0

Figure 3a shows the tendency of annual ET_0 on the TP. The annual average ET_0 was 1037.17 mm, ranging from 983.53 to 1091.94 mm from 1979 to 2018. The annual ET_0 experienced a non-significant ($\alpha = 0.05$) decrease by 2.1 mm/decade (Table 1). According to the Cramer's test, there are two abrupt change points in ET_0 series of TP, which are 1997 and 2000, respectively (Figure 3b). We found the decline rate of ET_0 was −25.9 mm/decade before 1997 and the change is significant, but the annual ET_0 increased significantly ($\alpha = 0.05$) at a rate of 31.1 mm/decade after 1997. Furthermore, the Cramer's test was also performed on all 73 stations to verify the representativeness of 1997, and the results showed that 41 of them could detect the mutation point in 1997. Therefore, it can represent the main mutation characteristics of ET_0 in the region. Since the variation of ET_0 is the result of the comprehensive effects of climate variables, it is necessary to analyze each climate variable during the two periods separately. Using the inflection point of ET_0 as the basis for dividing the period, all the time series of the 73 stations were divided in these two periods for the subsequent analysis.

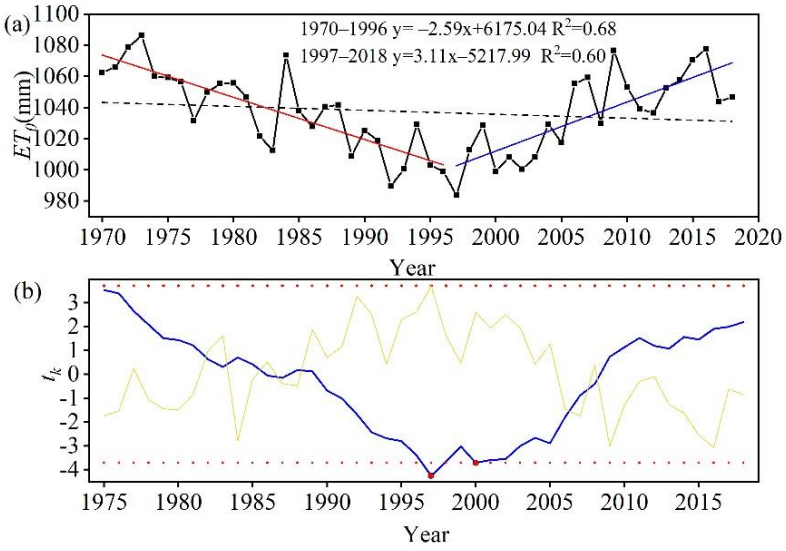

Figure 3. Variation of annual ET_0 (**a**) and Cramer's test results for detecting change in annual ET_0 (**b**) on the TP from 1970 to 2018. (The red points represent the years in which the mutation occurred in the ET_0 series.)

Table 1. Z value of reference evapotranspiration (ET_0), solar radiation (RS), relative humidity (RH), air temperature (T_{mean}) and wind speed (U_2) in different periods.

Period	*RS*	*RH*	T_{mean}	U_2	ET_0
1970–1996	0.08	3.13 *	2.54 *	−5.50 *	−4.84 *
1997–2018	−3.63 *	−3.63 *	2.48 *	4.32 *	3.80 *
1970–2018	−3.59 *	−1.08	6.54 *	−5.42 *	−1.20

* Statistically significant trends at the 5% significance level.

Figure 4 shows spatial distribution of ET_0 trends on the TP during 1970–1996 and 1997–2018. There were significant spatial differences in the trends of ET_0 before and after 1997. During 1970–1996, there are 52 stations showing a downward trend, and these downward trends were remarkable ($\alpha = 0.05$) at 34 meteorological stations; while 21 stations increased in the southeast TP from 1997 to 2018, there were annual ET_0 increasing trends at 49 meteorological stations, of which 36 meteorological stations increased significantly ($\alpha = 0.05$). Only 24 stations in the eastern TP showed a decreasing trend.

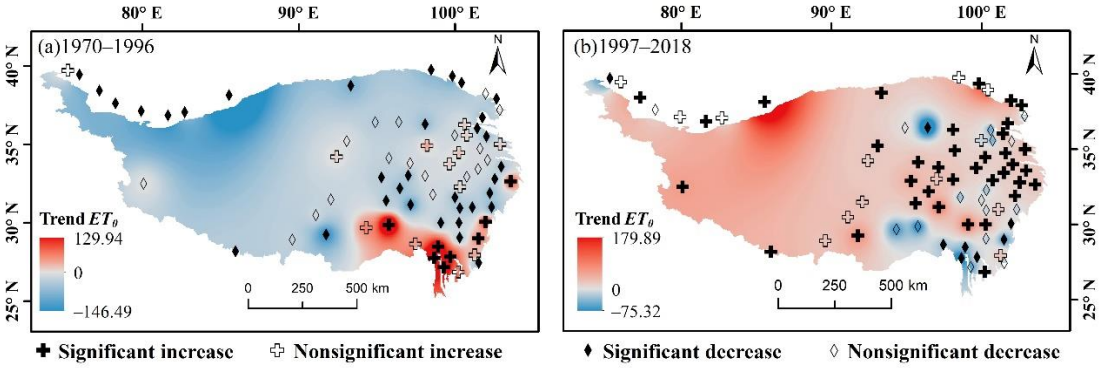

Figure 4. Spatial distribution of ET_0 trends on the TP during 1970–1996 (**a**) and 1997–2018 (**b**) (mm/10a).

3.2. Spatio-Temporal Variation Characteristics of Climatic Factors

Figure 5 and Table 1 shows the trends of climate variables on the TP from 1970 to 2018. The T_{mean} increased significantly ($\alpha = 0.05$) before and after 1997 at the rate of 0.125 and 0.373 °C/decade, respectively. The upward trend was steeper during the latter period than during the former period. *RS* and *RH* increased by 0.019 (MJ·m^{-2}·day^{-1})/decade and 1.68%/decade from 1970 to 1996 and decreased significantly at the rate of −0.163 (MJ·m^{-2}·day^{-1})/decade and −2.816%/decade after 1997, respectively. The variation of U_2 was opposite to the variation of *RS* and *RH*. U_2 decreased dramatically by 0.294 m/s/decade during the former period but increased significantly by 0.158 m/s/decade during the latter period.

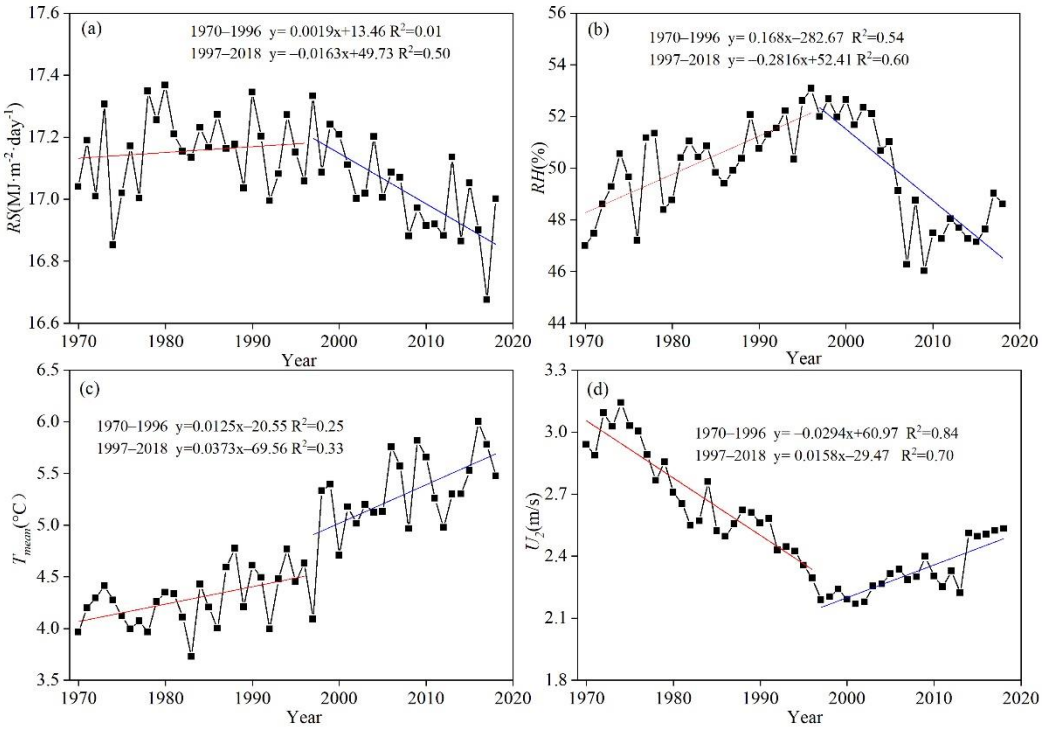

Figure 5. Annual variation of climatic factors on the TP during 1970–2018. (**a**) Solar radiation (*RS*); (**b**) relative humidity (*RH*); (**c**) air temperature (T_{mean}); (**d**) wind speed (U_2).

Figure 6 shows the spatial distribution of trends of four climate factors during 1970–1996 and 1997–2018. From 1970 to 1996, the increasing *RS* distributed partially in the southeast and west of the TP, and the decreasing *RS* majority distributed in the central area of the TP. From 1997 to 2018, the decreasing *RS* was found in most stations and the increasing *RS* distributed in some areas east and north-west of the TP. The increasing *RH* was found in most stations and the decreasing *RH* distributed in the north-western areas during 1970–1996, while the decreasing *RH* was found in most stations and the increasing *RH* distributed in some areas east of the TP during 1997–2018. T_{mean} increased across the entire area before and after 1996. From 1970 to 1996, U_2 showed a downward trend in most stations, while only a few stations in the eastern part of the plateau showed an increasing trend. However, from 1997 to 2018, U_2 of most stations showed an upward trend, and only a few stations decreased.

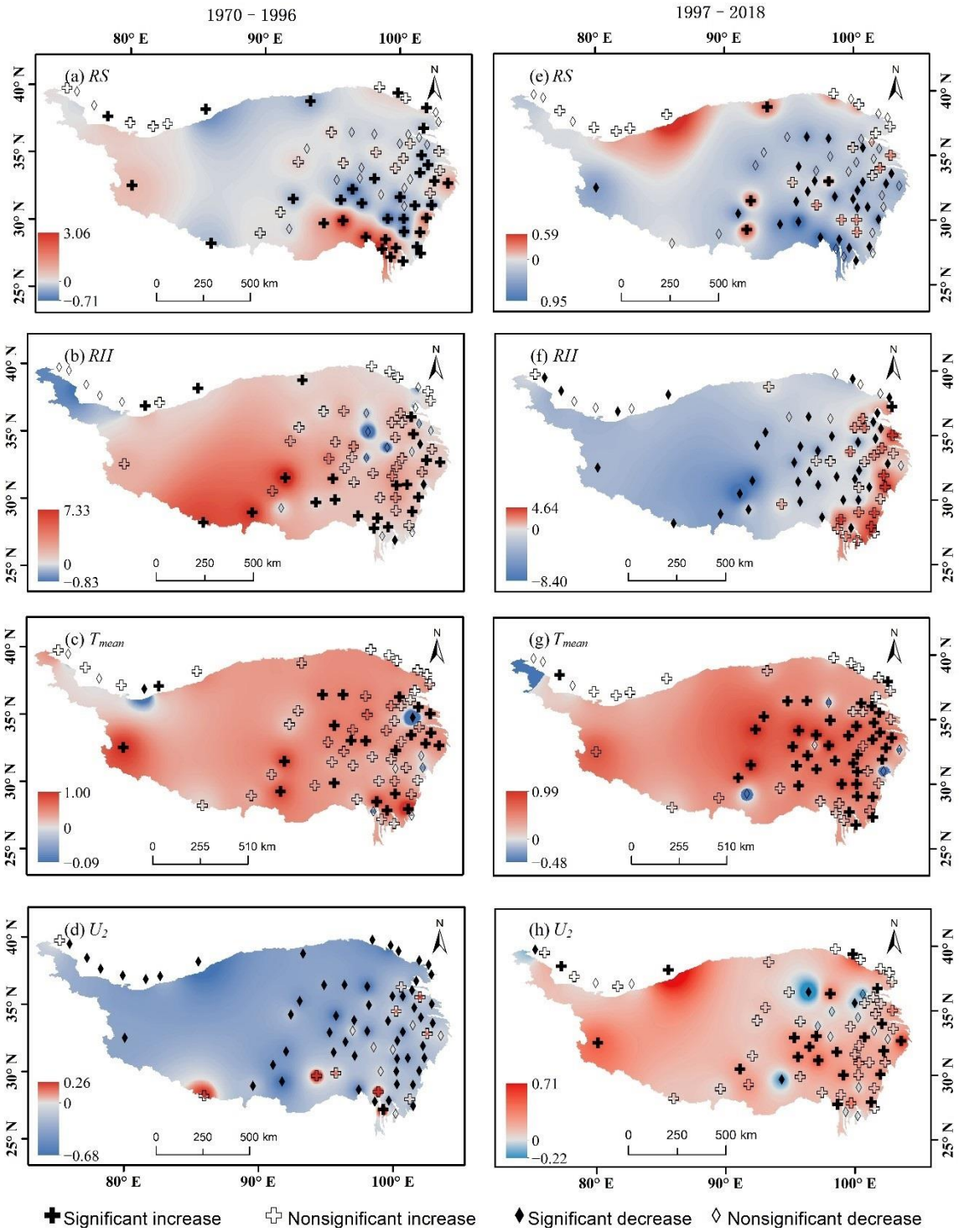

Figure 6. Spatial distribution of climatic factors trends during 1970–1996 (**a**–**d**) and 1997–2018 (**e**–**h**); (**a**,**e**) *RS* ((MJ m^{-2} day^{-1})/decade); (**b**,**f**) *RH* (%/decade); (**c**,**g**) T_{mean} (°C/decade); (**d**,**h**) U_2 (m/s/decade).

3.3. Spatial Distribution of the Sensitivity Coefficients

Figure 7 shows the spatial distribution of susceptibility coefficients on the TP. The sensitivity coefficient of *RS* (S_{RS}) ranged from 0.303 to 0.587 and decreased from southeast to northwest on the TP. The sensitivity coefficient of T_{mean} (S_{Tmean}) ranged from 0.025 to 0.172, which was similar to S_{RS}. Different from S_{RS} and S_{Tmean}, the sensitivity coefficient of U_2 (S_{U2}) increased progressively from southeast to northwest and varied from 0.080 to 0.259. The sensitivity coefficient of *RH* (S_{RH}) ranged from −0.444 to −0.019 and the

smallest absolute value of the S_{RH} found in the southeast corner of the TP and increases to the north. According to above discussion, the sensitivity of these four factors to the ET_0 on the TP was in the order: $S_{RS} > S_{RH} > S_{U2} > S_{Tmean}$.

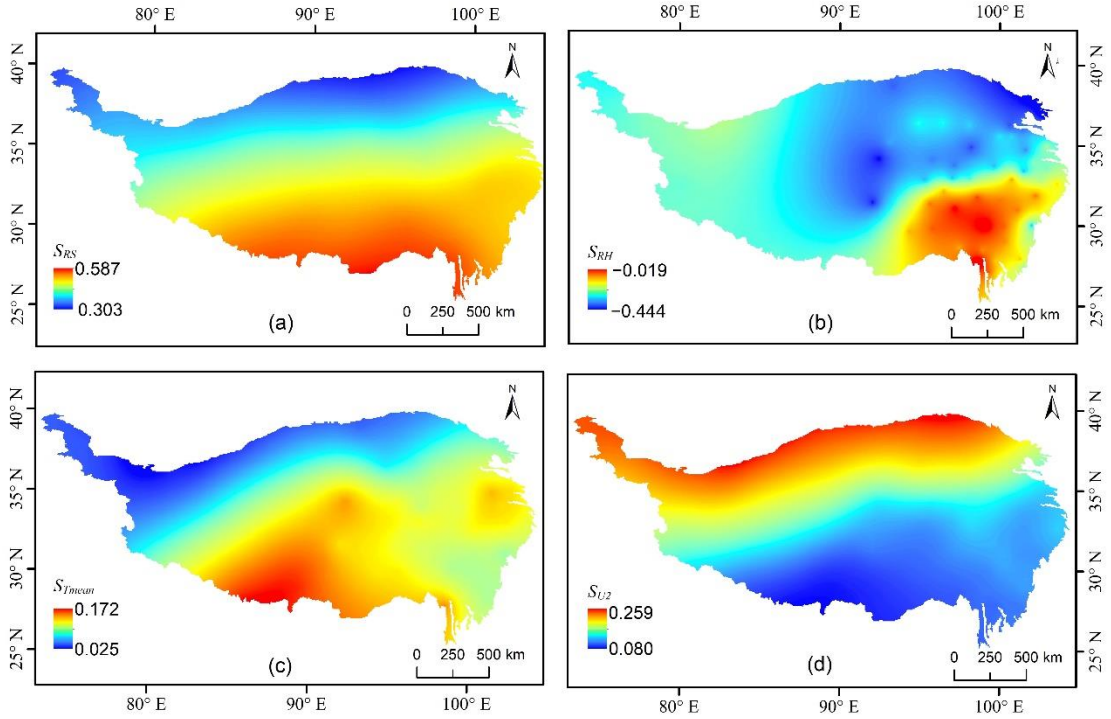

Figure 7. Spatial distribution of sensitivity coefficient on the TP during 1970–2018. (**a**) S_{RS}; (**b**) S_{RH}.; (**c**) S_{Tmean}; (**b**) S_{U2}.

3.4. Dominant Climate Factors of ET_0 Change

In order to identify the dominant climate factors affecting ET_0, the contribution rate of each climatic factor was calculated using Equation (11). Comparing the ET_0 trends caused by the four climate factors (C_ET_0) and the ET_0 trends calculated by P-M model (LR_ET_0), the relative errors were 12.79%, 4.70% and 7.93% during 1970–1996, 1997–2018 and 1970–2018, respectively (Table 2). Therefore, equation (11) was a reasonable method to estimate the contribution rates of the four climatic factors to ET_0.

Table 2. The contribution rate of climate factors to ET_0 in different periods (%).

Period	CR_{RS}	CR_{RH}	CR_{Tmean}	CR_{U2}	$C\_(ET_0)$	$LR\_(ET_0)$	ε
1970–1996	0.10	−2.43	0.80	−4.41	−5.94	−6.70	12.79
1997–2018	−0.96	3.33	1.58	2.34	6.29	6.60	4.70
1970–2018	−0.67	1.04	3.05	−4.29	−0.87	−0.94	7.93

Table 2 shows the contribution rate of the four climate factors to ET_0 in different periods. During 1970–1996, U_2 was the dominant factor influencing ET_0, followed by RH, T_{mean} and RS. The decrease of U_2 and increase of RH caused a −4.41% and −2.43% decrease to ET_0, respectively. However, the increases in T_{mean} and RS led to a 0.80% and 0.10% increase to ET_0, respectively. The comprehensive effect of climate factors finally led to a −6.7% decline to ET_0. During 1997–2018, the decrease of RH was the main reason causing the increase in ET_0 by 3.33%. In addition, the rise of U_2 and T_{mean} also aggravated the increase of ET_0 to a certain degree, resulting in the increase of ET_0 of 2.34% and 1.58%, respectively. The decrease of RS led to a variation in ET_0 of −0.96%. The effects of the climatic condition eventually caused the increase of ET_0 by 6.29%. In a word, the decrease of ET_0 during 1970 and 1996 was mainly due to the decrease of U_2, while the increase of ET_0 during 1997 and 2018 was mainly due to the decrease of RH.

Figure 8 gives the spatial distribution of contribution rates of four climatic factors to ET_0 during 1970–1996 and 1997–2018. From 1970 to 1996, the contribution rate of *RS* (CR_{RS}) was positive in the southeast and western TP, and the negative CR_{RS} was found in eastern and central parts of TP. From 1997 to 2018, CR_{RS} was mainly positive and the negative contribution distributed in the northern and central sporadic areas. The contribution rate of *RH* (CR_{RH}) was negative in most parts of TP and the positive CR_{RH} was only distributed partly in northwest and east before 1997; while, most regions on the TP exhibited a positive CR_{RH}, except some areas of eastern TP after 1997. The distribution of contribution rate of U_2 (CR_{U2}) was similar to that of *RH*. The contribution rate of T_{mean} (CRT_{mean}) was positive in most parts of TP during both periods.

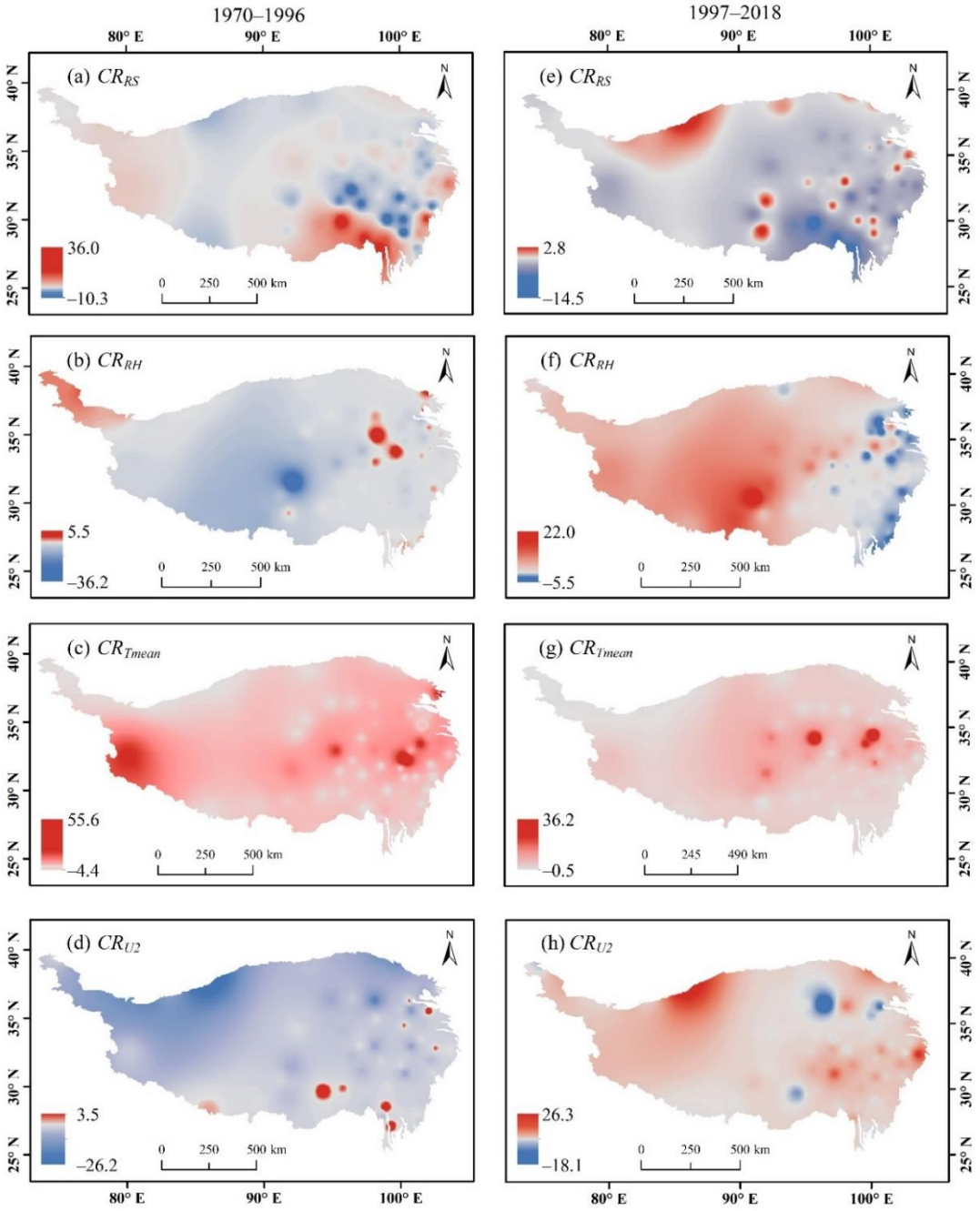

Figure 8. Spatial distribution of contribution rates of four climatic factors to ET_0 during 1970–1996 (**a**–**d**) and 1997–2018 (**e**–**h**) (%); (**a**,**e**) CR_{RS}; (**b**,**f**) CR_{RH}; (**c**,**g**) CRT_{mean}; (**d**,**h**) CR_{U2}.

4. Discussion

According to the analysis of this study, there are significant differences in climate factors between 1970–1996 and 1997–2018 (Figures 5 and 6; Table 1). The spatiotemporal dynamic of the four climate factors in this study is basically consistent with a lot of research on climatic change. Before 1997, the wind speed decreased significantly, but then increased significantly. The weakening of the Asian monsoon system may explicate the decrease of U_2 on the TP, while the strengthening of zonal wind may have a significant contribution to the increase of U_2 after 1997 [44]. An insignificantly decreasing trend of *RS* was found during 1970–1996, but a significantly decreasing trend was found during 1997–2018. The solar dimming over the TP is mainly caused by the increase in water vapor and deep cloud cover [3]. *RH* also decreased significantly after 1997. Most areas of TP belong to the arid region and the amount of water is limited. The rise of air temperature makes the saturated vapor pressure rise, which may be the reason for the decrease in *RH* [45]. The climatic factors and ET_0 have complex mutual feed mechanism and give rise to an abrupt change in ET_0 in the meantime.

ET_0 decreased significantly before 1997 while increased significantly after 1997 on the TP in this study (Figures 3 and 4; Table 1). The change of ET_0 is influenced by climate factors, and the weight of each climate factor is different. The dominant factor causing the decrease of ET_0 on the TP was U_2 before 1997(Figure 8; Table 2), and this is similar to many studies on the TP. For example, Chen et al. [46] found that wind speed is the dominant meteorological factor affecting the ET_0 of the TP. Zhang et al. [26] considered that wind speed caused changes in the ET_0 of the TP, especially in the northern part of the TP. Yin et al. [47] have shown that the decrease of wind speed can explain the variation of the potential annual evapotranspiration in the temperate zone of the north of China and the TP. In this study, the dominant factor that caused the increase of ET_0 on the TP after 1997 is *RH*, which is consistent with Wang's [27] study that relative humidity may be an important factor affecting ET_0. However, this is not consistent with the view of Xie Hong [48] that relative humidity is considered to have little effect. This is due to the difference in the research periods and methods.

Some uncertainties remain for the estimation of ET_0 in this study. Some of the parameters in the P-M equation are empirical and local. Therefore, regional optimization of parameters is an important means to improve the accuracy of ET_0 calculation. Additionally, the number of meteorological stations used in this study is limited and unevenly distributed. The TP has large area and complex natural environment. It is difficult to fully describe the spatiotemporal dynamic of the climatic factors and ET_0. More data from different sources and interpolation methods should be introduced in the future.

5. Conclusions

In this study, we analyzed the temporal–spatial trends, transition characteristics of ET_0 and identified the main reasons for the change of ET_0 in different stages over the TP based on data from 73 weather stations during 1970–2018.The main conclusions are:

1. There is an abrupt point in the TP's annual ET_0 series around 1997. The ET_0 decreased remarkably at a rate of −25.9 mm/decade before 1997, while increasing significantly at a speed of 31.1 mm/decade after 1997;
2. Second item: before 1997, T_{mean} and *RH* increased significantly while U_2 decreased significantly and *RS* decreased insignificantly. After 1997, T_{mean} and U_2 increased insignificantly, *RH* and *RS* decreased significantly;
3. The sensitivity analysis of each climate factor to ET_0 indicated the ET_0 on the TP is most sensitive to *RS*, followed by *RH*, U_2 and T_{mean};
4. Third item: from 1970 to 1996, U_2 was the most important meteorological factor contributing to the decline of ET_0, followed by *RH*, T_{mean}, and *RS*. During 1997–2018, the decreasing of *RH* was the dominant factor causing an increase in ET_0. The increase of U_2 and T_{mean} also intensified the increase of ET_0 to a certain extent.

Author Contributions: Conceptualization, S.H. and T.Z.; data curation, R.G.; formal analysis, R.G.; funding acquisition, S.H.; methodology, P.B.; resources, T.Z.; visualization, R.Z.; writing—original draft, S.H. and R.G.; writing—review and editing, S.H., T.Z., P.B. and R.Z. All authors have read and agreed to the published version of the manuscript.

Funding: This research was funded by National Natural Science Foundation of China, grant number 41501027, the Beijing Outstanding Young Scientist Program, grant number BJJWZYJH01201910028032.

Institutional Review Board Statement: Not applicable.

Informed Consent Statement: Not applicable.

Data Availability Statement: There are no relevant statements for this research.

Acknowledgments: The authors would like to express their sincere thanks to National Natural Science Foundation of China (41501027) and Beijing Outstanding Young Scientist Program (BJJWZYJH01201910028032) for their valuable support. The authors also would like to thank the peer reviewers for their valuable suggestions and comments on improving this paper.

Conflicts of Interest: The authors declare no conflict of interest.

References

1. Lu, X.; Zang, C.; Burenina, T. Study on the variation in evapotranspiration in different period of the Genhe River Basin in China. *Phys. Chem. Earth* **2020**, *120*, 102902. [CrossRef]
2. Maeda, E.E.; Wiberg, D.A.; Pellikka, P.K.E. Estimating reference evapotranspiration using remote sensing and empirical models in a region with limited ground data availability in Kenya. *Appl. Geogr.* **2011**, *31*, 251–258. [CrossRef]
3. Kun, Y.; Baohong, D.; Jun, Q.; Wenjun, T.; Ning, L.; Changgui, L. Can aerosol loading explain the solar dimming over the Tibetan Plateau? *Geophys. Res. Lett.* **2012**, *39*. [CrossRef]
4. Boisier, J.P.; de Noblet-Ducoudré, N.; Ciais, P. Historical land-use-induced evapotranspiration changes estimated from present-day observations and reconstructed land-cover maps. *Hydrol. Earth Syst. Sci.* **2014**, *18*, 3571–3590. [CrossRef]
5. Wu, H.; Wang, X.; Wang, Y.; Xu, Y.; Han, X. Temporal variations in reference evapotranspiration in Hubei Province, China, from 1960 to 2014. *Theor. Appl. Climatol.* **2019**, *135*, 433–448. [CrossRef]
6. Liu, C.; Zhang, D. Temporal and Spatial Change Analysis of the Sensitivity of Potential Evapotranspiration to Meteorological Influencing Factorsin China. *Acta Geogr. Sin.* **2011**, *66*, 579–588.
7. Rachid, H.; Tarik, B.; Hayat, L.; Adil, S. Comparative assessment of different reference evapotranspiration models towards a fit calibration for arid and semi-arid areas. *J. Arid Environ.* **2021**, *184*, 104318.
8. Zhao, J.; Xia, H.; Yue, Q.; Wang, Z. Spatiotemporal variation in reference evapotranspiration and its contributing climatic factors in China under future scenarios. *Int. J. Climatol.* **2020**, *40*, 3813–3831. [CrossRef]
9. Fan, J.; Wu, L.; Zhang, F.; Xiang, Y.; Zheng, J. Climate change effects on reference crop evapotranspiration across different climatic zones of China during 1956–2015. *J. Hydrol.* **2016**, *542*, 923–937. [CrossRef]
10. Li, Y.; Wei, X.; Su, H. Quantitative analysis of causes for temporal and spatial variation characteristics and evolution of potential evapotranspiration in Gansu Province during recent 30 years. *J. Water Resour. Water Eng.* **2015**, *26*, 219–225.
11. Wang, Z.; Ye, A.; Wang, L.; Liu, K.; Cheng, L. Spatial and temporal characteristics of reference evapotranspiration and its climatic driving factors over China from 1979–2015. *Agric. Water Manag.* **2019**, *213*, 1096–1108. [CrossRef]
12. Liu, X.; Zheng, H.; Zhang, M.; Liu, C. Identification of dominant climate factor for pan evaporation trend in the Tibetan Plateau. *J. Geogr. Sci.* **2011**, *21*, 594–608. [CrossRef]
13. Deepak, J.; Yagob, D.; Ercan, K.; Vijay, P.S.; Ahmad, F.F. Trends in reference evapotranspiration in the humid region of northeast India. *Hydrol. Process.* **2012**, *26*, 421–435.
14. Michael, L.R.; Graham, D.F. Changes in New Zealand pan evaporation since the 1970s. *Int. J. Climatol.* **2005**, *25*, 2031–2039.
15. Moonen, A.C.; Ercoli, L.; Mariotti, M.; Masoni, A. Climate change in Italy indicated by agrometeorological indices over 122 years. *Agric. For. Meteorol.* **2002**, *111*, 13–27. [CrossRef]
16. Brutsaert, W.; Parlange, M.B. Hydrologic cycle explains the evaporation paradox. *Nat. Int. Wkly. J. Sci.* **1998**, *396*, 30. [CrossRef]
17. Han, J.; Wang, J.; Zhao, Y.; Wang, Q.; Zhang, B.; Li, H.; Zhai, J. Spatio-temporal variation of potential evapotranspiration and climatic drivers in the Jing-Jin-Ji region, North China. *Agric. For. Meteorol.* **2018**, *256*, 75–83. [CrossRef]
18. Xu, S.; Yu, Z.; Yang, C.; Ji, X.; Zhang, K. Trends in evapotranspiration and their responses to climate change and vegetation greening over the upper reaches of the Yellow River Basin. *Agric. For. Meteorol.* **2018**, *263*, 118–129. [CrossRef]
19. Zhang, Q.; Wang, W.; Wang, S.; Zhang, L. Increasing Trend of Pan Evaporation over the Semiarid Loess Plateau under a Warming Climate. *J. Appl. Meteorol. Clim.* **2016**, *55*, 2007–2020. [CrossRef]
20. Brij, K.P.; Deepak, K. Identification of trend in long term precipitation and reference evapotranspiration over Narmada river basin (India). *Glob. Planet. Chang.* **2018**, *161*, 172–182.
21. Cong, Z.T.; Yang, D.W.; Ni, G.H. Does evaporation paradox exist in China? *Hydrol. Earth Syst. Sci. Discuss.* **2008**, *5*, 357–366.

22. Liu, X.; Zhang, D.; Luo, Y.; Liu, C. Spatial and temporal changes in aridity index in northwest China: 1960 to 2010. *Theor. Appl. Climatol.* **2013**, *112*, 307–316. [CrossRef]
23. Zhang, S.; Li, X.; Zhao, G.; Huang, Y. Surface energy fluxes and controls of evapotranspiration in three alpine ecosystems of Qinghai Lake watershed, NE Qinghai-Tibet Plateau. *Ecohydrology* **2016**, *9*, 267–279. [CrossRef]
24. Duan, A.; Xiao, Z. Does the climate warming hiatus exist over the Tibetan Plateau? *Sci. Rep.* **2015**, *5*, 13711. [CrossRef]
25. You, Q.; Kang, S.; Fluegel, W.; Pepin, N.; Yan, Y.; Huang, J. Decreasing wind speed and weakening latitudinal surface pressure gradients in the Tibetan Plateau. *Clim. Res.* **2010**, *42*, 57–64. [CrossRef]
26. Zhang, X.; Ren, Y.; Yin, Z.; Lin, Z.; Zheng, D. Spatial and temporal variation patterns of reference evapotranspiration across the Qinghai-Tibetan Plateau during 1971–2004. *J. Geophys. Res.* **2009**, *114*, D1505. [CrossRef]
27. Wang, B.; Zhang, X. Reference Evapotranspiration and Its Attribution on the Tibetan Plateau from 1971 to 2014. *Arid Zone Res.* **2019**, *36*, 4–14.
28. Jiang, Y.; Wang, P.; Xu, X.; Zhang, J. Dynamics of carbon fluxes with responses to vegetation, meteorological and terrain factors in the south-eastern Tibetan Plateau. *Environ. Earth Sci.* **2014**, *72*, 4551–4565. [CrossRef]
29. Cui, M.; Wang, J.; Wang, S.; Yan, H.; Li, Y. Temporal and Spatial Distribution of Evapotranspiration and Its Influencing Factors on Qinghai-Tibet Plateau from 1982 to 2014. *J. Resour. Ecol.* **2019**, *10*, 213–224.
30. Allen, R.G.; Pereira, L.S.; Raes, D.; Smith, M. *Crop Evapotranspiration: Guidelines for Computing Crop Water Requirements*; Food and Agricultural Organization: Rome, Italy, 1998; p. 56.
31. Zheng, H.; Liu, X.; Liu, C.; Dai, X.; Zhu, R. Assessing contributions to panevaporation trends in Haihe River Basin, China. *J. Geophys. Res. Atmos.* **2009**, *114*, D24. [CrossRef]
32. Gao, X.; Zhao, Q.; Zhao, X.; Wu, P.; Pan, W.; Gao, X.; Sun, M. Temporal and spatial evolution of the standardized precipitation evapotranspiration index (SPEI) in the Loess Plateau under climate change from 2001 to 2050. *Sci. Total Environ.* **2017**, *595*, 191–200. [CrossRef]
33. Robert, M.H.; James, R.S. A Nonparametric Trend Test for Seasonal Data With Serial Dependence. *Water Resour. Res.* **1984**, *20*, 727–732.
34. Huang, J.; Liu, F.; Xue, Y.; Sun, S. The spatial and temporal analysis of precipitation concentration and dry spell in Qinghai, northwest China. *Stoch. Environ. Res. Risk A* **2015**, *29*, 1403–1411. [CrossRef]
35. Gillard, J. Circular and Linear Regression: Fitting Circles and Lines by Least Squares. *J. R. Stat. Soc. Ser. A* **2011**, *174*, 843. [CrossRef]
36. Nalder, I.A.; Wein, R.W. Spatial interpolation of climatic Normals: Test of a new method in the Canadian boreal forest. *Agric. For. Meteorol.* **1998**, *92*, 211–225. [CrossRef]
37. Lin, Z.H.; Mo, X.G.; Li, H.X.; Li, H.B. Comparison of three spatial interpolation methods for climate variables in China. *Acta Geogr. Sin.* **2002**, *57*, 47–56.
38. Beven, K. A sensitivity analysis of the Penman-Monteith actual evapotranspiration estimates. *J. Hydrol.* **1979**, *44*, 169–190. [CrossRef]
39. Liu, X.; Zheng, H.; Liu, C.; Cao, Y. Sensitivity of the Potential Evapotranspiration to Key Climatic Variables in the Haihe River Basin. *Resour. Sci.* **2009**, *31*, 1470–1476.
40. Mccuen, R.H. A sensitivity and error analysis Cf procedures used for estimating evaporation. *J. Am. Water Resour. Assoc.* **1974**, *10*, 486–497. [CrossRef]
41. Lenhart, T.; Eckhardt, K.; Fohrer, N.; Frede, H.G. Comparison of two different approaches of sensitivity analysis. *Phys. Chem. Earth* **2002**, *27*, 645–654. [CrossRef]
42. Yin, Y.; Wu, S.; Dai, E. Determining factors in potential evapotranspiration changes over China in the period 1971–2008. *Chin. Sci. Bull.* **2010**, *55*, 3329–3337. [CrossRef]
43. Li, Y.; Liang, K.; Bai, P.; Feng, A.; Liu, L.; Dong, G. The spatiotemporal variation of reference evapotranspiration and the contribution of its climatic factors in the Loess Plateau, China. *Environ. Earth Sci.* **2016**, *75*, 364. [CrossRef]
44. Zhang, Z.; Yang, Y.; Zhang, X.; Chen, Z. Wind speed changes and its influencing factors in Southwestern China. *Acta Ecol. Sin.* **2014**, *34*, 471–481.
45. Chen, S.; Liu, Y.; Axel, T. Climatic change on the Tibetan Plateau: Potential Evapotranspiration Trends from 1961–2000. *Clim. Chang.* **2006**, *76*, 291–319.
46. Xie, X.; You, Q.; Lin, H. Surface relative humidity decreases and its cause over the Qinghai—Tibetan Plateau in recent ten years. *Plateau Meteorol.* **2018**, *37*, 642–650.
47. Yin, Y.; Wu, S.; Chen, G.; Dai, E. Attribution analyses of potential evapotranspiration changes in China since the 1960s. *Theor. Appl. Climatol.* **2010**, *101*, 19–28. [CrossRef]
48. Xie, H. *The Evapotranspiration and Its Response to Climate Change in Tibet Plateau*; Lanzhou University: Lanzhou, China, 2012.